J|A|C|S
JOURNAL OF THE AMERICAN CHEMICAL SOCIETY

pubs.acs.org/JACS

Article

Crystalline Arrays of Copper Porphyrin Qubits Based on Ion-Paired Frameworks

Casandra M. Moisanu,† Robert M. Jacobberger,† Luke P. Skala,† Charlotte L. Stern,
Michael R. Wasielewski,* and William R. Dichtel*

Cite This: *J. Am. Chem. Soc.* 2023, 145, 18447−18454

Read Online

ACCESS | Metrics & More | Article Recommendations | Supporting Information

ABSTRACT: Molecular electronic spin qubits have great potential for use in quantum information science applications because their structure can be rationally tuned using synthetic chemistry. Their integration into a new class of materials, ion-paired frameworks, allows for the formation of ordered arrays of these molecular spin qubits. Three ion-paired frameworks with varying densities of paramagnetic Cu(II) porphyrins were isolated as micron-sized crystals suitable for characterization by single-crystal X-ray diffraction. Pulse-electron paramagnetic resonance (EPR) spectroscopy probed the spin coherence of these materials at temperatures up to 140 K. The crystals with the longest Cu−Cu distances had a spin−spin relaxation time (T_m) of 207 ns and a spin−lattice relaxation time (T_1) of 1.8 ms at 5 K, which decreased at elevated temperature because of spin−phonon coupling. Crystals with shorter Cu−Cu distances also had lower T_1 values because of enhanced cross-relaxation from qubit−qubit dipolar coupling. Frameworks with shorter Cu−Cu distances exhibited lower T_m values because of the increased interactions between qubits within the frameworks. Incorporating molecular electronic spin qubits in ion-paired frameworks enables control of composition, spacing, and interqubit interactions, providing a rational means to extend spin relaxation times.

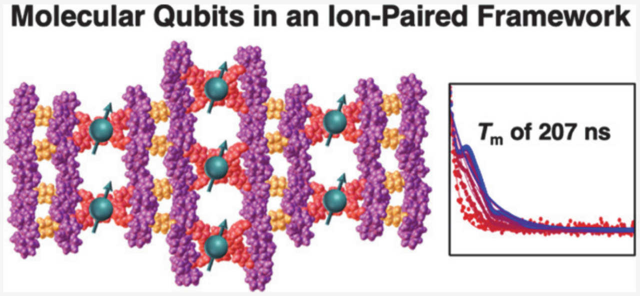

INTRODUCTION

Quantum information science (QIS) takes advantage of materials that can obtain a quantum superposition state, which is of interest for quantum computing, quantum cryptography, and quantum sensing.[1−3] These efforts rely on the development of the quantum bit, or qubit,[4,5] and numerous qubit candidates have been studied, including trapped ions,[6] quantum dots,[7] and nitrogen-vacancy centers in diamond.[8−10] Molecules with unpaired electrons can also function as qubits and have the potential of being designed and tuned using synthetic and physical chemical principles.[4,11−14] Furthermore, it is now increasingly possible to design solid-state molecular assemblies to order qubits into extended arrays with emergent properties. Several types of supramolecular assemblies can incorporate molecular spins, including metal−organic frameworks (MOFs)[1,15−18] or two-dimensional polymers (2DPs).[19] The promise of these approaches is to tune qubit coupling, and especially their spin−lattice (T_1) and spin−spin (T_m) relaxation times.[14]

Framework materials are promising candidates for organizing qubits into periodic arrays.[17,18] In pioneering work, Freedman and co-workers reported a $Cu_{1.0}$-PCN-224 MOF with a T_m of 46 ns at 10 K,[18] which was increased to 52 ns in an isostructural MOF with larger Cu spacings.[17] T_m values in MOFs were further increased by incorporating small numbers of paramagnetic qubits into a matrix of isostructural diamagnetic analogues, which increases the average interqubit distance. Changing the MOF structure from one in which 100% of porphyrins contain a Cu^{2+} qubit to one in which the Cu^{2+} ions were found in 10% of the porphyrins, with the other 90% of porphyrins containing a diamagnetic metal ion, resulted in an increase of T_m from 46 to 645 ns.[18] However, these increased T_m values are achieved with an accompanying loss of structural precision of the assembly, which may be problematic for applications that rely on the precise spacing of qubits within the spin array.[14,20,21] These factors motivated us to explore new approaches to noncovalent assembly that provide structural precision, high materials quality, full incorporation of qubits, and longer qubit spacings. Furthermore, it might also prove advantageous that the ideal supramolecular platform for hosting qubit candidates be composed of light elements with small spin−orbit coupling and elements with a high natural abundance of isotopes that lack a nuclear spin.

Received: May 8, 2023
Published: August 8, 2023

https://doi.org/10.1021/jacs.3c04786
J. Am. Chem. Soc. 2023, 145, 18447−18454

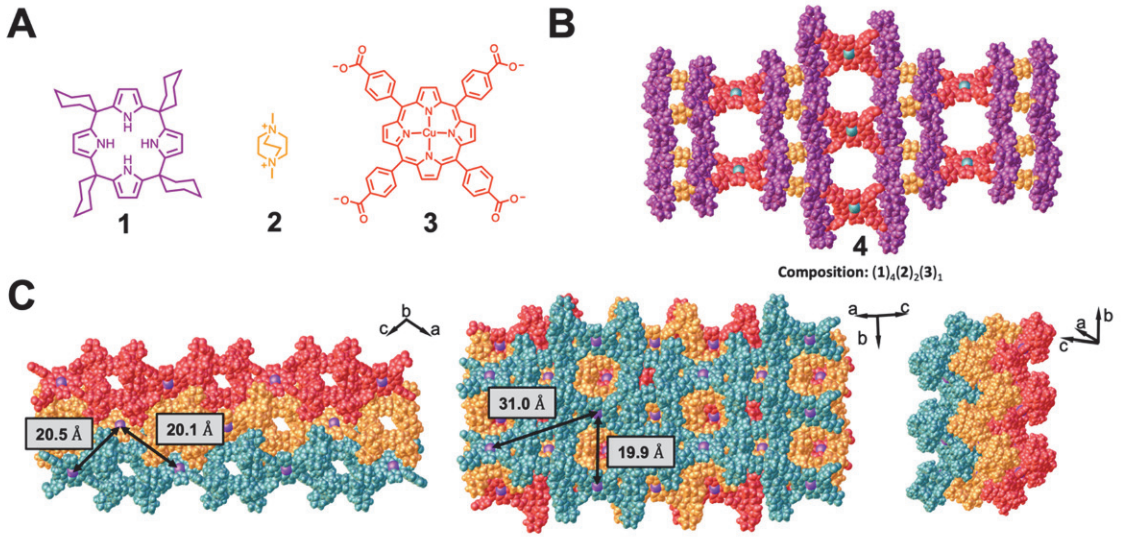

Figure 1. (A) Building blocks found in **4**. (B) Single-crystal X-ray structure of **4**. Solvent molecules have been removed for clarity. (C) Single-crystal X-ray structures depicting stacking of three layers (teal, orange, red) in the assembly. Different crystallographic orientations demonstrate an offset stacking of the supramolecular sheets as well as different pore sizes. Atomic distances highlight the distance between Cu ions in the structure. The 19.9 Å distance marked in the figure is the shortest distance between copper ions in the structure.

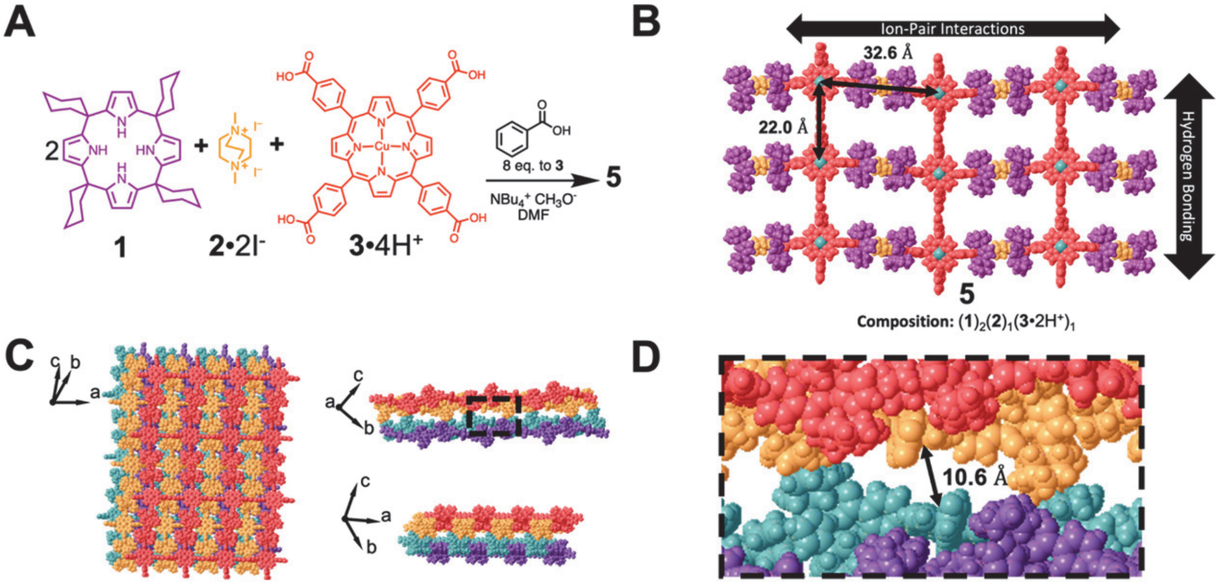

Figure 2. (A) Reaction scheme for the crystallization of network **5**. (B) Single-crystal X-ray structure of **5**. Solvent molecules have been removed for clarity. Ion-pair host−guest interactions between **1**, **2**, and **3** run horizontally through the structure as shown, while hydrogen bonding interactions run vertically through the structure in between the carboxylates of $\mathbf{3}{\cdot}2H^+$. (C) Single-crystal X-ray structures depicting stacking of four layers (purple, teal, orange, red) in the assembly. Different crystallographic orientations demonstrate an offset stacking of the supramolecular sheets as well as different pore sizes. (D) Enlarged view of the gap between two layers of sheets corresponding to the dashed box in C. The distance between the stacked pair of sheets is 10.6 Å, which is the shortest distance between two Cu atoms in the crystal structure.

Ion-paired frameworks are a recently introduced class of crystalline organic solids, which employ the host−guest chemistry of tetrakis(spirocyclohexane)calix[4]pyrrole (C4P, **1**)[22−24] to direct the crystallization of organic anions and cations into low-density, periodic materials.[25,26] Their structures are composed of organic building blocks with low spin−orbit coupling and nuclear spin, which pose minimal interference with the electron spin qubits.[14,27,28] Multiple ions and macrocyclic hosts have been crystallized into two-dimensional assemblies, one-dimensional assemblies, and supramolecular ladder polymers,[25] all of which were characterized by single-crystal X-ray diffraction (SCXRD). These characteristics are desirable for ordering molecular spin qubits into arrays. Here, we pair a Cu porphyrin-based molecular qubit, Cu(II)-tetrakis(4-carboxyphenyl)porphyrin (CuTCPP, $\mathbf{3}{\cdot}4H^+$) with two dicationic linkers, dimethyl-1,4-diazabicyclo[2.2.2]octane (DM-DABCO, $\mathbf{2}{\cdot}2I^-$), and methyl viologen ($\mathbf{6}{\cdot}2I^-$), along with C4P (**1**) to provide three assemblies (**4**, **5**, and **7**) with variable qubit spacings. Pulse-electron paramagnetic resonance (EPR) spectroscopy indicates that these crystalline assemblies have long T_m values compared to porphyrin-containing MOFs with complete occupancy of Cu^{2+} ions. These results will motivate future studies of ion-

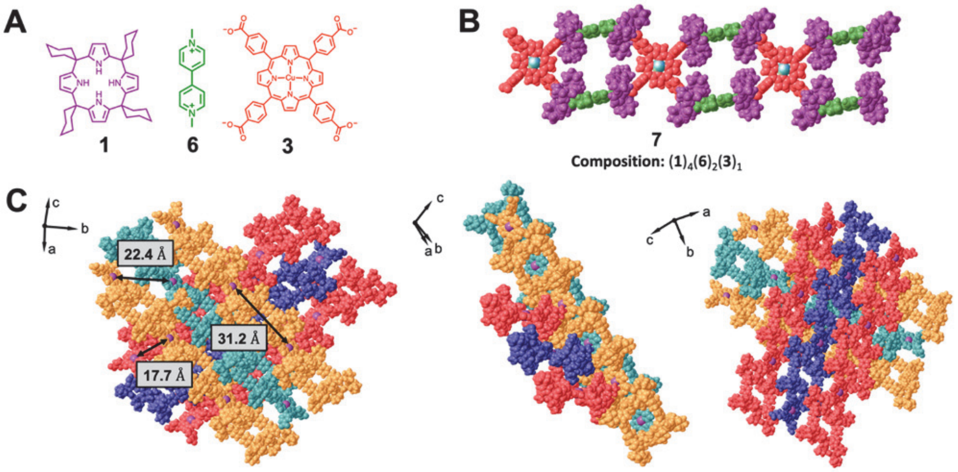

Figure 3. (A) Building blocks found in **7**. (B) Single-crystal X-ray structure of **7**. Solvent molecules have been removed for clarity. (C) Single-crystal X-ray structure depicting six ladder polymers in the assembly. Different crystallographic orientations demonstrate an offset stacking of the ladder polymers. Atomic distances highlight the distance between Cu atoms (colored in purple) in the structure. The shortest distance between Cu atoms is 17.7 Å which occurs between alternating ladder polymer layers.

paired frameworks as a promising strategy to design concentrated qubit arrays with long T_m values.

■ RESULTS AND DISCUSSION

C4P (**1**), DM-DABCO ($\mathbf{2}\cdot 2I^-$), and CuTCPP ($\mathbf{3}\cdot 4H^+$) assemble to form crystals suitable for SCXRD when dissolved in dimethylformamide (DMF) in the presence of the base, tetrabutylammonium methoxide (4 equiv relative to $\mathbf{3}\cdot 4H^+$). **1** simultaneously binds carboxylate and quaternary ammonium ions (Figure 1A), ultimately resulting in the assembly and crystallization of layered 2D lattices defined by the directionality of the ion-pair recognition elements as monoclinic single crystals (**4**). SCXRD revealed copper porphyrins each binding to four C4Ps through multidentate NH−O hydrogen bonding interactions between the C4P N−H bonds and the aryl carboxylate ions. Two molecules of **2** complete the unit cell by binding within an electron-rich pocket on the opposite sides of the C4Ps, resulting in an empirical composition of $(\mathbf{1})_4(\mathbf{2})_2(\mathbf{3})_1$ that crystallizes with 14 disordered molecules of the DMF solvent (Figure 1B). The solvent-masking procedure implemented in Olex2 was used to remove the electron contribution of disordered solvent molecules in this and all other crystal structures reported here. Further analysis of the ion pairing interactions of **2** and **3** revealed these assemblies to be composed of 2D sheets that stack in an offset geometry (Figure 1C, left). Within each sheet, rows of copper porphyrins tilt 45° offset to the plane of the sheet, causing the sheets to adopt a zig-zag structure (Figure 1C, right panel). As a consequence of these arrangements, **4** has small pores within each layer that are visible along the b and c axes (Figure 1C, left and middle, and Figure 1B). Based on the single-crystal XRD structure, each Cu^{2+} ion within one sheet has six nearest neighbors (Figure 1B): four Cu^{2+} ions are 31.0 Å and two Cu^{2+} ions are 19.9 Å away, which is the shortest $Cu^{2+}-Cu^{2+}$ distance in the structure (Figure 1C). Having successfully crystallized **4** and recognizing the value of establishing the relationship between structure and spin relaxation behavior in these materials (see below), we explored alternative CuTCPP-based networks based on ion-pair recognition and other noncovalent interactions.

By performing the crystallization in the presence of benzoic acid to control the rate of crystal growth, a different framework was formed, which was also characterized using SCXRD. This material has distinct $Cu^{2+}-Cu^{2+}$ spacings relative to **4** and was crystallized under the same conditions as **4** but in the presence of benzoic acid (8 equiv relative to $\mathbf{3}\cdot 4H^+$, Figure 2A). These conditions provided triclinic rod-shaped crystals **5** (Figure 2B) with different stoichiometry and noncovalent interactions relative to **4**. In **5**, only two C4Ps bind to each CuTCPP in a trans configuration. Similar to **4**, the dication **2** connects two C4Ps to provide a linear ion-pair recognition-based assembly (shown horizontally in Figure 2B). The other two carboxylic acids of each CuTCPP do not bind C4Ps; instead, they form hydrogen-bonded dimers with the free carboxylic acids of a neighboring porphyrin. These hydrogen bonding interactions run perpendicular to the ion-pair interactions (in the vertical direction in Figure 2B), resulting in two-dimensional sheets based on linear arrangements of distinct noncovalent interactions that run along perpendicular directions. The composition of **5** is therefore deficient in **1** and **2** relative to **4**, corresponding to an empirical formula of $(\mathbf{1})_2(\mathbf{2})_1(\mathbf{3}\cdot 2H^+)_1\cdot 3$ DMF (Figure 2B). In one sheet, the Cu^{2+} ions in **5** in the direction of the carboxylic acid dimers are 22.0 Å apart, while the Cu^{2+} ions along the direction of the interactions between **1**, **2**, and $\mathbf{3}\cdot 2H^+$ are 32.6 Å apart (Figure 2B). The sheets of **5** stack in an A−B fashion (Figure 2C), such that the CuTCPPs in adjacent layers are fully offset from one another. Figure 2C shows two stacked pairs (one red and orange, the other teal and purple) of sheets of **5** from three crystallographic orientations. This stacking mode results in the shortest copper−copper distance observed in any crystal lattice in this study at 10.6 Å. This distance occurs between pairs of sheets and can be seen in Figure 2D as the gap between the orange and teal sheets in the crystal structure.

The $Cu^{2+}-Cu^{2+}$ distances were varied while maintaining the design principles of **4** by using a larger dication, methyl viologen ($\mathbf{6}\cdot 2I^-$) in place of **2** (Figure 3A). The resulting assembly **7** was crystallized under similar conditions as **4** by dissolving the monomers in DMF and adding tetrabutylammonium methoxide as a base. Monoclinic crystals of **7** were isolated and solved by SCXRD. Rather than forming 2D sheets as observed in **4**, the monomers in **7** form supramolecular ladder polymers with an empirical formula of $(\mathbf{1})_4(\mathbf{6})_2(\mathbf{3})_1\cdot$DMF (Figure 3B), yet these ladder polymers achieve similar intralayer $Cu^{2+}-Cu^{2+}$ distances compared to **4** (Figure 3C). The binding arrangement of **1**, **3**, and a dication typically occurs in a colinear fashion, as observed in assemblies **4** and **5**. In **7**, the C4Ps bind **6** in an alternate, side-on geometry, which allows the C4Ps to adopt a nonlinear arrangement and form supramolecular ladder polymers instead of two-dimensional networks. These ladder polymers stack in alternating sheets, forming a crisscross pattern in the crystal structure (Figure 3C), which gives rise to the shortest distance between two copper centers of 17.7 Å between two ladder polymers (Figure 3C).

The viability of the frameworks as atomically ordered arrays of spin qubits was assessed using EPR spectroscopy, which enabled the characterization of the spin properties and spin dynamics of the qubit ensembles. All measurements were taken on samples containing an ensemble of single crystals of either **4**, **5**, or **7**. Continuous-wave (CW) EPR spectroscopy was conducted on **4**, **5**, and **7** at 5 K (red spectra in Figure 4), and the CW-EPR spectra were fit[29] using EasySpin 5.2.35 (blue spectra in Figure 4) to extract the spin Hamiltonian parameters, including the g-tensor, hyperfine interactions, and linewidths (Table S1). The electronic structure of the copper(II) porphyrins is relatively unperturbed after being incorporated into the frameworks, as the axial *g*-tensors and axial hyperfine interactions are consistent with those found previously in solid solutions containing isolated, noninteracting copper(II) porphyrins.[30−32] The Lorentzian linewidths, Γ_L, in **4** (0.06 mT) and **7** (0.06 mT) are significantly narrower than that in **5** (1.0 mT), indicating that electron−electron dipolar interactions are weaker in the two former frameworks. This weaker dipolar coupling is likely due to the lower spin density and longer spin nearest-neighbor distances in **4** and **7** and also yields longer spin coherence times, as demonstrated below. We note that the Γ_L in **4** and **7** are also narrower than that in atomically precise qubit arrays based on copper(II) porphyrins assembled into MOFs, as reported in Yu et al.[17,18]

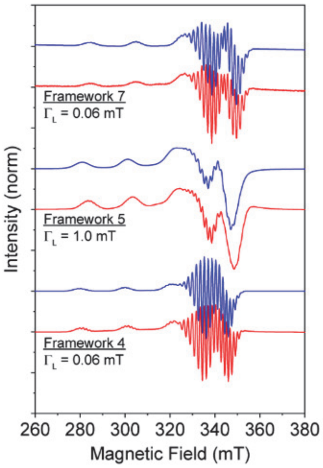

Figure 4. CW-EPR spectra of **4**, **5**, and **7** (bottom to top) collected at 5 K, in which the experimental data and best-fit simulations are shown in red and blue, respectively. Lorentzian (Γ_L) linewidths of the simulated spectra are provided, which are related to electron−electron dipolar coupling.

The qubit ensembles in **4**, **5**, and **7** were manipulated using pulse-EPR spectroscopy to demonstrate coherent quantum control (Figure 5) and probe their spin dynamics as a function of temperature (Figure 6). The effect of the orientation of the Cu^{2+} spin centers was also elucidated by conducting the pulse-EPR experiments at varying magnetic fields, which enables specific molecular orientations to be selectively addressed because of the anisotropic Cu^{2+} electronic structure. The transition at the lower magnetic field around 290 mT corresponds to the principal axis $g_{\parallel}$, which is perpendicular to the porphyrin plane, whereas the transition at the higher magnetic field around 330 mT corresponds to a powder average of orientations that is dominated by the principal axis $g_{\perp}$, which is parallel to the porphyrin plane (Figure S1).

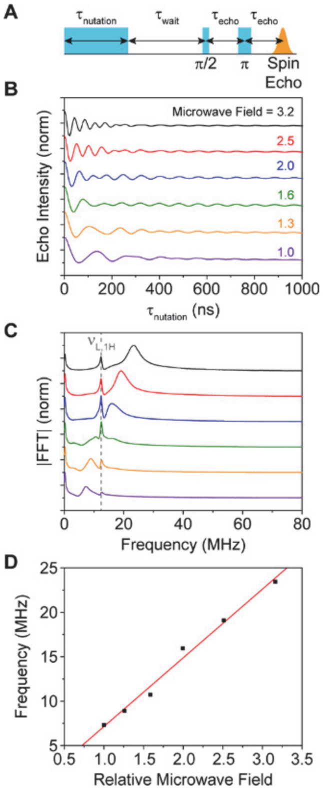

Figure 5. (A) Pulse sequence in which τ_{nutation} is varied to detect Rabi oscillations. (B) Variable-power nutation data for **4** at 292.0 mT and 5 K, demonstrating Rabi oscillations. (C) Fast Fourier transform (FFT) of Rabi oscillations and (D) Rabi oscillation frequency versus relative microwave field strength. Larmor frequency of ^1H is indicated in (C) with a gray dashed line.

Coherent quantum control over the qubits in **4**, **5**, and **7** was demonstrated at 5 K by driving Rabi oscillations (Figures 5B and S2) using a nutation pulse sequence (Figure 5A). As the duration of the nutation pulse, τ_{nutation}, increases, the echo intensity oscillates. This oscillating intensity is due to rotation of the spins between the $m_s = -1/2$ and $+1/2$ sublevels, which are located at opposite poles of the Bloch sphere, where local extrema correspond to $m_s = -1/2$ and $+1/2$ and all other points correspond to superpositions of $m_s = -1/2$ and $+1/2$. The Rabi oscillations therefore establish that the qubits can be placed into an arbitrary superposition of these two quantum states. The Rabi oscillation frequency, Ω_{Rabi}, which quantifies the time, $\tau_{\text{spin-flip}} = (2\Omega_{\text{Rabi}})^{-1}$, required to perform a logic gate

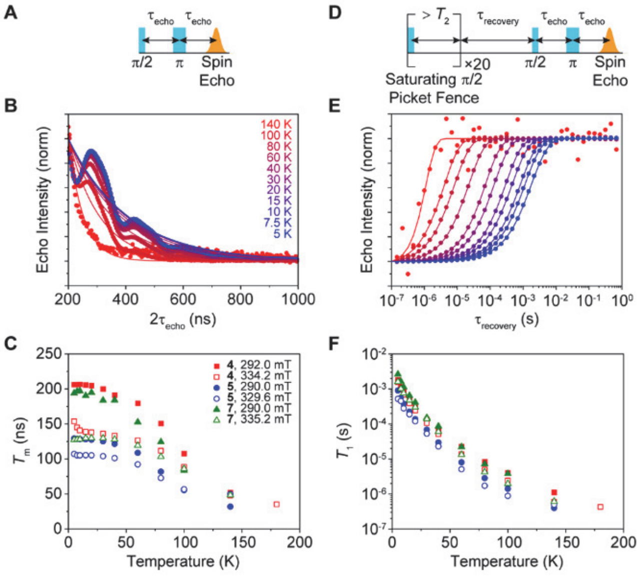

Figure 6. Pulse sequences in which (A) τ_{echo} and (D) τ_{recovery} are varied to measure T_{m} and T_1, respectively. Representative variable-temperature (B) Hahn-echo data and (E) saturation recovery data from which T_{m} and T_1 are extracted, respectively, for **4** at 292.0 mT. (C) T_{m} and (F) T_1 versus temperature for **4** (red squares), **5** (blue circles), and **7** (green triangles) at magnetic fields corresponding to $g_{\parallel}$ (smaller field, solid symbols) and $g_{\perp}$ (larger field, open symbols). The reproducibility of the T_{m} data is shown in Figure S4.

that flips the spins between the two quantum states, is determined from Fourier analysis of the nutation data (Figures 5C and S2). The spins are flipped faster with increasing microwave power (Figures 5D and S2), and the Rabi frequency scales linearly with microwave field strength as expected for an $S = 1/2$ spin center.[33] For example, for **4**, $\tau_{\text{spin-flip}}$ decreases from 68 to 21 ns when the microwave field strength increases by a factor of 3.2. The Fourier analysis also reveals a peak (e.g., located at 12.4 MHz for **4** at 292.0 mT) that does not shift with microwave power, which is discussed further below.

For the qubit ensembles within each framework, we characterized the phase memory lifetime, T_{m}, which is among the most important qubit performance metrics because it defines the time frame in which all quantum gate operations must be performed. T_{m} encompasses all processes contributing to spin decoherence, including the intrinsic dephasing lifetime (T_2), spectral diffusion, and instantaneous diffusion. T_{m} is determined by measuring the echo intensity as a function of the interpulse delay time, τ_{echo}, (Figure 6B) within a two-pulse Hahn-echo sequence (Figure 6A) and fitting the data to the monoexponential function $I(2\tau_{\text{echo}}) = A_0 \exp(-2\tau_{\text{echo}}/T_{\text{m}}) + A_1$, where A_0 and A_1 are constants.

The dependence of T_{m} on crystal structure, molecular orientation, and temperature revealed that electron−electron dipolar coupling and hyperfine interactions are the dominant sources of spin decoherence in the frameworks. Between 5 and 140 K, T_{m} increases from **5** to **7** to **4**, T_{m} is larger at $g_{\parallel}$ than at $g_{\perp}$, and T_{m} generally decreases with increasing temperature (Figure 6C). For example, at 10 K and at the $g_{\parallel}$ transition, the T_{m} of **5**, **7**, and **4** are 128, 197, and 207 ns, respectively. We attribute this trend to the decreasing spin density per unit cell (0.196, 0.162, and 0.142 spins nm^{-3}, respectively) and the increasing Cu^{2+} nearest-neighbor distance (10.6, 17.7, 19.9 Å, respectively) from **5** to **7** to **4**. We conclude that the reduced spin density leads to weaker dipolar coupling between nearby qubits and yields longer T_{m}, as has previously been found in qubits embedded within MOFs and 2DPs.[1,17,19]

Hyperfine coupling of the qubits to nearby ^1H nuclear spins also contributes to decoherence. Fourier analysis of the Rabi oscillations (Figures 5C and S2) collected at 5 K at the $g_{\parallel}$ and $g_{\perp}$ transitions revealed a peak at 12.4 and 14.1 MHz, respectively. These peaks, which do not shift with microwave power, match the Larmor frequency, υ_{L}, of ^1H nuclear spins, indicating that qubit interactions with ^1H give rise to electron spin-echo envelope modulation (ESEEM). In assemblies **4** and **7**, there are 100 and 174 ^1H atoms within 4 to 10 Å around Cu^{2+} ions, respectively. Assembly **5** has two distinct Cu^{2+} centers that have 95 and 58 ^1H atoms within that same range. This ESEEM is also observed in the echo decay curves obtained using two-pulse (Figures 6B, S3, and S4) and three-pulse (Figure S5) Hahn-echo sequences. The ESEEM oscillations in Figures 6B, S3, and S4 become less intense as the spin density increases from **4** to **7** to **5** and as the temperature increases. These data therefore indicate that the contribution of hyperfine interactions to decoherence increases as the spin density decreases and temperature decreases. Conversely, the contribution of dipolar coupling to decoherence increases as the spin density increases. Interestingly, ESEEM from ^{14}N nuclear spins is not observed—which is likely a result of their proximity to and strong coupling with the qubits[34]—indicating that hyperfine coupling of the qubits to ^{14}N is not a major source of decoherence.

For each framework and molecular orientation, T_{m} is nearly constant between 5 and 30 K and decreases roughly linearly with temperature above 40 K (Figure 6C). The temperature independence of T_{m} below 30 K is consistent with decoherence due to dipolar or hyperfine interactions. We attribute the reduction in T_{m} above 40 K to the motion of rotatable bonds, for example, from methyl groups in DMF that is incorporated into the crystal structure of the frameworks.[19,28,35] The measured T_{m} of 207 ns (151 ns) at 10 K (80 K) in **4** is 4.0× (6.4×) larger than the longest T_{m} reported in an atomically precise molecular qubit array.[17] Even at the highest temperature studied here of 140 K, spin−lattice relaxation is still not the dominant source of decoherence, as the spin−lattice relaxation lifetime, T_1, is 10−20 times larger than T_{m}. For quantum applications, it is highly desirable to achieve long T_{m} at high temperatures, preferably above 77 K so that liquid nitrogen, which is relatively inexpensive and abundant compared to liquid helium, can be used to cool the qubit devices during operation.

We attribute the longer T_{m} at the $g_{\parallel}$ transition than that at the $g_{\perp}$ transition for **4**, **5**, and **7** (Figure 6C) to the smaller number of on-resonant Cu^{2+} sites near each qubit that contribute to decoherence at $g_{\parallel}$. For example, at $g_{\perp}$, the microwave pulses address more porphyrin orientations within the sample (because $g_{\perp}$ roughly corresponds to a powder average of the g_x, g_y, and g_z transitions), which means that more of the Cu^{2+} sites near qubits are on-resonant and contribute to decoherence. In contrast, at $g_{\parallel}$, the microwave pulses address fewer porphyrin orientations (because $g_{\parallel}$ corresponds solely to the g_z transition), which means that more of the Cu^{2+} sites near qubits are off-resonant (i.e., the Cu^{2+} sites that have porphyrin planes that are rotated with respect to those of on-resonant Cu^{2+} sites) and contribute less strongly to decoherence.

Next, we characterized T_1, which is the time frame in which the spins relax to their thermal ground state, as described by Boltzmann statistics, and provides the upper limit for T_2. T_1 is determined by measuring the echo intensity as a function of the recovery time, τ_{recovery}, (Figure 6E) within a saturation recovery pulse sequence (Figure 6D). The saturation recovery curves are fit with the stretched exponential functions $I(\tau_{\text{recovery}}) = 1 - A_0 \exp\left(-(\tau_{\text{recovery}}/T_1)^{\beta}\right) + A_1$, where A_0 and A_1 are constants and β is the stretch factor that is used to assess the dominant contributions to spin−lattice relaxation, as described below.

As temperature increases and spin density increases, T_1 is reduced due to increased spin−phonon coupling and increased cross-relaxation from qubit−qubit dipolar coupling, respectively.[18] For example, T_1 at $g_{\parallel}$ of **4** is 1.8×10^{-3}, 1.3×10^{-4}, 2.3×10^{-5}, and 1.1×10^{-6} s at 5, 30, 60, and 140 K, respectively. Moreover, between 5 and 140 K, T_1 of **4** and **7** are similar, typically differing by <40%, whereas T_1 of **5** is significantly smaller than that of **4** and **7**, typically by a factor of 2.5−3.0. The measured T_1 in **7** of 1.1×10^{-3} s (7.1×10^{-6} s) at 10 K (80 K) is 2.1× (4.7×) larger than the longest T_1 reported in an atomically precise molecular qubit array.[17]

The sources of spin−lattice relaxation and their dependence on temperature and spin density are elucidated from the value of β. When $\beta = 1$, the saturation recovery data is described by a monoexponential decay curve and relaxation is purely mediated by phonons. When β approaches 0.5, a second process also mediates relaxation, which is attributed to cross-relaxation. At $g_{\parallel}$ of **4** and **7**, β is >0.86 and >0.83, respectively, at all temperatures between 5 and 140 K, indicating that spin−phonon coupling is the dominant source of spin−lattice relaxation. In contrast, in **5**, β is 0.56 at 5 K and increases with increasing temperature, although it never exceeds 0.8, indicating that cross-relaxation contributes more significantly to spin−lattice relaxation. The increased importance of cross-relaxation in **5** compared to **4** and **7** is consistent with the higher spin density, lower T_m, and larger Γ_L in the former system. For each framework, β generally increases with increasing temperature, which is expected due to increased spin−phonon coupling at higher temperatures.

The T_m at $g_{\parallel}$ of **4** was increased from 206 to 580 ns (Figure 7B) at 5 K by using a Carr−Purcell−Meiboom−Gill (CPMG) pulse sequence (Figure 7A), in which a train of microwave π pulses is applied after the $\pi/2$ pulse in the Hahn-echo sequence, to dynamically decouple the qubits from nearby electronic or nuclear spins. An oscillatory dependence of T_m on τ_{CPMG} is observed at 292.0 mT (Figure 7C) and 332.4 mT (Figure S6). At each transition, the oscillations exhibit two components, marked with * and + symbols in Figures 7C and S6B, that have different relative amplitudes but the same frequency of 12.8 and 14.0 MHz at 292.0 and 332.4 mT, respectively. These frequencies closely match the Larmor frequency of ^{1}H nuclear spins at each respective transition, which was also observed in the Fourier analysis of the Rabi oscillations in Figures 5C and S2. Therefore, we conclude that the CPMG pulse sequence primarily decouples the qubits from nearby ^{1}H nuclear spins, where each set of oscillations marked with * or + is due to ^{1}H with different hyperfine coupling to the qubits. These data further highlight the importance of reducing the density of spin-active nuclei within the frameworks. In particular, deuterating the porphyrin molecules or DMF solvent to substitute ^{1}H with ^{2}H is a promising route to reduce the hyperfine coupling and increase T_m, as ^{2}H has a lower gyromagnetic ratio than ^{1}H by a factor of 6.5.

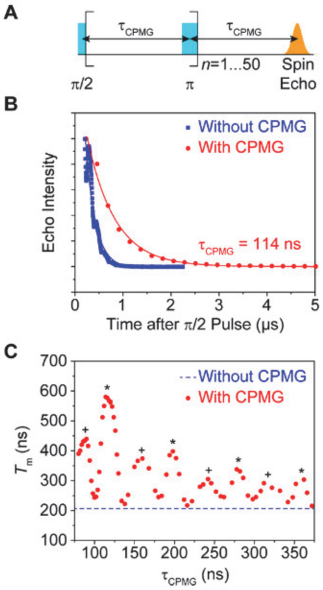

Figure 7. (A) Pulse sequence used to measure T_m via the CPMG method. (B) Coherence decay curves obtained using a two-pulse Hahn echo (blue) and a CPMG (red) pulse sequence (with interpulse delay time, τ_{CPMG}, of 114 ns) for **4** at 292.0 mT and 5 K, from which T_m of 206 and 580 ns, respectively, are extracted. (C) Plot of the oscillatory dependence of T_m on τ_{CPMG} for **4** at 292.0 mT and 5 K. The two sets of peaks, each with a periodicity of 12.8 MHz, are indicated with * and + symbols.

■ CONCLUSIONS

Ion-paired frameworks organize Cu porphyrin molecular qubits with tunable control of their spacing. A combination of the design of the dication monomer and crystallization conditions resulted in the formation of distinct supramolecular 2D and ladder polymer structures. Each of these solids has different Cu porphyrin density and Cu−Cu distances, and frameworks with lower spin density minimize qubit−qubit dipolar coupling and thereby suppress decoherence. Ultimately, these characteristics resulted in enhanced T_m for the framework with the lowest spin density, **4**, with a T_m of 207 ns at 10 K. This value is currently the longest T_m for a framework material whose spin-active groups were not diluted statistically with a structurally similar closed shell monomer. The relatively long spin coherence properties of the ion-paired frameworks arise in part from their atomic composition, high degree of modularity, and high materials quality. This assembly strategy is likely expandable to additional two- and three-dimensional topologies, which would offer other means to control interqubit distances. This work points the way forward to designing new types of networks to further improve the spin properties of these systems.

■ ASSOCIATED CONTENT

Supporting Information

The Supporting Information is available free of charge at https://pubs.acs.org/doi/10.1021/jacs.3c04786.

Materials and instrumentation, synthetic procedures, single-crystal X-ray diffraction of frameworks, EPR characterization of frameworks, and ^{1}HNMR spectra of monomers (PDF)

Accession Codes

CCDC 2251275−2251277 contain the supplementary crystallographic data for this paper. These data can be obtained free of charge via www.ccdc.cam.ac.uk/data_request/cif, or by emailing data_request@ccdc.cam.ac.uk, or by contacting The Cambridge Crystallographic Data Centre, 12 Union Road, Cambridge CB2 1EZ, UK; fax: +44 1223 336033.

AUTHOR INFORMATION

Corresponding Authors

Michael R. Wasielewski − *Department of Chemistry, Northwestern University, Evanston, Illinois 60208, United States;* orcid.org/0000-0003-2920-5440; Email: m-wasielewski@northwestern.edu

William R. Dichtel − *Department of Chemistry, Northwestern University, Evanston, Illinois 60208, United States;* orcid.org/0000-0002-3635-6119; Email: wdichtel@northestern.edu

Authors

Casandra M. Moisanu − *Department of Chemistry, Northwestern University, Evanston, Illinois 60208, United States;* orcid.org/0000-0001-8760-9991

Robert M. Jacobberger − *Department of Chemistry, Northwestern University, Evanston, Illinois 60208, United States;* orcid.org/0000-0001-5947-5308

Luke P. Skala − *Department of Chemistry, Northwestern University, Evanston, Illinois 60208, United States;* orcid.org/0000-0003-4914-5414

Charlotte L. Stern − *Department of Chemistry, Northwestern University, Evanston, Illinois 60208, United States;* orcid.org/0000-0002-9491-289X

Complete contact information is available at: https://pubs.acs.org/10.1021/jacs.3c04786

Author Contributions

[†]C.M.M., R.M.J., and L.P.S. contributed equally to this work.

Notes

The authors declare no competing financial interest.

ACKNOWLEDGMENTS

L.P.S. was supported by a NSF Graduate Research Fellowship under grant DGE-1842165. C.M.M. is supported by a NSF Graduate Research Fellowship under grant DGE-2234667. This work made use of the Integrated Molecular Structure Education and Research Center (IMSERC) at Northwestern University, which has received support from the NSF (CHE-1048773), the Soft and Hybrid Nanotechnology Experimental (SHyNE) Resource (NSF; NNCI-1542205), the State of Illinois, the International Institute for Nanotechnology (IIN), and the National Science Foundation under award # CHE-2154627 (M.R.W.).

REFERENCES

(1) Yamabayashi, T.; Atzori, M.; Tesi, L.; Cosquer, G.; Santanni, F.; Boulon, M.-E.; Morra, E.; Benci, S.; Torre, R.; Chiesa, M.; Sorace, L.; Sessoli, R.; Yamashita, M. Scaling up electronic spin qubits into a three-dimensional metal−organic framework. *J. Am. Chem. Soc.* **2018**, *140*, 12090−12101.

(2) Laorenza, D. W.; Kairalapova, A.; Bayliss, S. L.; Goldzak, T.; Greene, S. M.; Weiss, L. R.; Deb, P.; Mintun, P. J.; Collins, K. A.; Awschalom, D. D.; et al. Tunable Cr4+ Molecular Color Centers. *J. Am. Chem. Soc.* **2021**, *143*, 21350−21363.

(3) Wasielewski, M. R.; Forbes, M. D. E.; Frank, N. L.; Kowalski, K.; Scholes, G. D.; Yuen-Zhou, J.; Baldo, M. A.; Freedman, D. E.; Goldsmith, R. H.; Goodson, T.; et al. Exploiting chemistry and molecular systems for quantum information science. *Nat. Rev. Chem.* **2020**, *4*, 490−504.

(4) Ladd, T. D.; Jelezko, F.; Laflamme, R.; Nakamura, Y.; Monroe, C.; O'Brien, J. L. Quantum computers. *Nature* **2010**, *464*, 45−53.

(5) Dowling, J. P.; Milburn, G. J. Quantum technology: the second quantum revolution. *Philos. Trans. R. Soc. A* **2003**, *361*, 1655−1674.

(6) Ozeri, R. The trapped-ion qubit tool box. *Contemp. Phys.* **2011**, *52*, 531−550.

(7) Kloeffel, C.; Loss, D. Prospects for Spin-Based Quantum Computing in Quantum Dots. *Annu. Rev. Condens. Matter Phys.* **2013**, *4*, 51−81.

(8) Childress, L.; Hanson, R. Diamond NV centers for quantum computing and quantum networks. *MRS Bull.* **2013**, *38*, 134−138.

(9) Doherty, M. W.; Manson, N. B.; Delaney, P.; Jelezko, F.; Wrachtrup, J.; Hollenberg, L. C. L. The nitrogen-vacancy colour centre in diamond. *Phys. Rep.* **2013**, *528*, 1−45.

(10) Bar-Gill, N.; Pham, L. M.; Jarmola, A.; Budker, D.; Walsworth, R. L. Solid-state electronic spin coherence time approaching one second. *Nat. Commun.* **2013**, *4*, 1743.

(11) Troiani, F.; Affronte, M. Molecular spins for quantum information technologies. *Chem. Soc. Rev.* **2011**, *40*, 3119−3129.

(12) Awschalom, D. D.; Bassett, L. C.; Dzurak, A. S.; Hu, E. L.; Petta, J. R. Quantum spintronics: engineering and manipulating atom-like spins in semiconductors. *Science* **2013**, *339*, 1174−1179.

(13) Zadrozny, J. M.; Niklas, J.; Poluektov, O. G.; Freedman, D. E. Millisecond Coherence Time in a Tunable Molecular Electronic Spin Qubit. *ACS Cent. Sci.* **2015**, *1*, 488−492.

(14) Graham, M. J.; Zadrozny, J. M.; Fataftah, M. S.; Freedman, D. E. Forging Solid-State Qubit Design Principles in a Molecular Furnace. *Chem. Mater.* **2017**, *29*, 1885−1897.

(15) Furukawa, H.; Cordova, K. E.; O'Keeffe, M.; Yaghi, O. M. The Chemistry and Applications of Metal-Organic Frameworks. *Science* **2013**, *341*, No. 1230444.

(16) Eddaoudi, M.; Moler, D. B.; Li, H.; Chen, B.; Reineke, T. M.; O'Keeffe, M.; Yaghi, O. M. Modular Chemistry: Secondary Building Units as a Basis for the Design of Highly Porous and Robust Metal−Organic Carboxylate Frameworks. *Acc. Chem. Res.* **2001**, *34*, 319−330.

(17) Yu, C.-J.; von Kugelgen, S.; Krzyaniak, M. D.; Ji, W.; Dichtel, W. R.; Wasielewski, M. R.; Freedman, D. E. Spin and Phonon Design in Modular Arrays of Molecular Qubits. *Chem. Mater.* **2020**, *32*, 10200−10206.

(18) Yu, C.-J.; Krzyaniak, M. D.; Fataftah, M. S.; Wasielewski, M. R.; Freedman, D. E. A concentrated array of copper porphyrin candidate qubits. *Chem. Sci.* **2019**, *10*, 1702−1708.

(19) Oanta, A. K.; Collins, K. A.; Evans, A. M.; Pratik, S. M.; Hall, L. A.; Strauss, M. J.; Marder, S. R.; D'Alessandro, D. M.; Rajh, T.; Freedman, D. E.; et al. Electronic Spin Qubit Candidates Arrayed within Layered Two-Dimensional Polymers. *J. Am. Chem. Soc.* **2023**, *145*, 689−696.

(20) Richardson, C. J. K.; Lordi, V.; Misra, S.; Shabani, J. Materials science for quantum information science and technology. *MRS Bull.* **2020**, *45*, 485−497.

(21) DiVincenzo, D. P. The Physical Implementation of Quantum Computation. *Fortsch. Phys.* **2000**, *48*, 771−783.

(22) Kim, D. S.; Sessler, J. L. Calix[4]pyrroles: versatile molecular containers with ion transport, recognition, and molecular switching functions. *Chem. Soc. Rev.* **2015**, *44*, 532−546.

(23) Kim, S. K.; Sessler, J. L. Calix[4]pyrrole-Based Ion Pair Receptors. *Acc. Chem. Res.* **2014**, *47*, 2525−2536.

(24) Gale, P. A.; Sessler, J. L.; Král, V.; Lynch, V. Calix[4]pyrroles: Old Yet New Anion-Binding Agents. *J. Am. Chem. Soc.* **1996**, *118*, 5140−5141.

(25) Skala, L. P.; Aguilar-Enriquez, X.; Stern, C. L.; Dichtel, W. R. Dissipative crystallization of ion-pair receptors. *Chem* **2023**, *9*, 709−720.

(26) Skala, L. P.; Stern, C. L.; Bancroft, L.; Moisanu, C. M.; Pelkowski, C.; Aguilar-Enriquez, X.; Swartz, J. L.; Wasielewski, M. R.; Dichtel, W. R. A modular platform for the precise assembly of molecular frameworks composed of ion pairs. *Chem* **2023**, *9*, 1208−1220.

(27) Wolfe, J. P. Direct Observation of a Nuclear Spin Diffusion Barrier. *Phys. Rev. Lett.* **1973**, *31*, 907−910.

(28) Berliner, L. J.; Eaton, G. R.; Eaton, S. S. Distance Measurements in Biological Systems by EPR. In *Biological magnetic resonance*; 2002.

(29) Stoll, S.; Schweiger, A. EasySpin, a comprehensive software package for spectral simulation and analysis in EPR. *J. Magn. Reson.* **2006**, *178*, 42−55.

(30) Shao, J.; Steene, E.; Hoffman, B. M.; Ghosh, A. EPR, ENDOR, and DFT Studies on (*β*-Octahalo-meso-tetraarylporphyrin)copper Complexes: Characterization of the Metal(d)−Porphyrin(a2u) Orbital Interaction. *Eur. J. Inorg. Chem.* **2005**, *2005*, 1609−1615.

(31) Greiner, S. P.; Rowlands, D. L.; Kreilick, R. W. EPR and ENDOR study of selected porphyrin- and phthalocyanine-copper complexes. *J. Phys. Chem.* **1992**, *96*, 9132−9139.

(32) Cunningham, K. L.; McNett, K. M.; Pierce, R. A.; Davis, K. A.; Harris, H. H.; Falck, D. M.; McMillin, D. R. EPR Spectra, Luminescence Data, and Radiationless Decay Processes of Copper(II) Porphyrins. *Inorg. Chem.* **1997**, *36*, 608−613.

(33) Akhtar, W.; Sekiguchi, T.; Itahashi, T.; Filidou, V.; Morton, J. J. L.; Vlasenko, L.; Itoh, K. M. Rabi oscillation and electron-spin-echo envelope modulation of the photoexcited triplet spin system in silicon. *Phys. Rev. B* **2012**, *86*, No. 115206.

(34) Graham, M. J.; Yu, C.-J.; Krzyaniak, M. D.; Wasielewski, M. R.; Freedman, D. E. Synthetic Approach To Determine the Effect of Nuclear Spin Distance on Electronic Spin Decoherence. *J. Am. Chem. Soc.* **2017**, *139*, 3196−3201.

(35) von Kugelgen, S.; Krzyaniak, M. D.; Gu, M.; Puggioni, D.; Rondinelli, J. M.; Wasielewski, M. R.; Freedman, D. E. Spectral Addressability in a Modular Two Qubit System. *J. Am. Chem. Soc.* **2021**, *143*, 8069−8077.

https://doi.org/10.1021/jacs.3c04786
J. Am. Chem. Soc. 2023, 145, 18447−18454